

Size scaling of the addition spectra in silicon quantum dots

M. Boehm, M. Hofheinz, X. Jehl, and M. Sanquer*
CEA-DRFMC, 17 rue des Martyrs, F-38054 Grenoble, France

M. Vinet, B. Previtali, D. Fraboulet, D. Mariolle, and S. Deleonibus
CEA-DRT-LETI, 17 rue des Martyrs F-38054 Grenoble Cedex 9, France

(Received 21 September 2004; revised manuscript received 27 October 2004; published 5 January 2005)

We investigate small artificial quantum dots obtained by geometrically controlled resistive confinement in low mobility silicon-on-insulator nanowires. Addition spectra were recorded at low temperature for various dot areas fixed by lithography. We compare the standard deviation of the addition spectra with theory in the high electron concentration regime. We find that the standard deviation scales as the inverse area of the dot and its absolute value are comparable to the energy spacing of the one-particle spectrum.

DOI: 10.1103/PhysRevB.71.033305

PACS number(s): 73.23.Hk, 73.63.-b

Measuring the current as a function of gate voltage provides decisive information on the addition spectrum of electrons in quantum dots. The addition energy is given by $\Delta_2(N) = E_{N+1} + E_{N-1} - 2E_N = e\alpha\delta V_g(N)$, where $\delta V_g(N)$ is the difference in gate voltage between the N^{th} and the $(N+1)^{\text{th}}$ current resonance, $\alpha = C_g/C_\Sigma$ is the ratio between the gate and total capacitance of the dot, and E_N is the ground-state energy of the N -electron state.¹ Few experiments concentrate on the fluctuations of the addition energy, $\sigma_2 = \sqrt{\langle \Delta_2^2 \rangle - \langle \Delta_2 \rangle^2}$, which require a large number of resonances to be measured.²⁻⁶ The distribution of Δ_2 found in experiments is generally close to a Gaussian with a standard deviation σ_2 varying from values comparable to the mean one-particle level spacing Δ_1 to much larger values. Until now the statistical variation of addition spectra was studied in dots made with high mobility two-dimensional (2D) electron gases with a large $k_F\ell$ parameter, where k_F is the Fermi wave vector and ℓ the elastic mean-free path. The size of the dots varied by orders of magnitude between the different experiments. On the theoretical side, addition spectra have attracted considerable interest. Restricting ourselves to the case of a large number, N , of electrons, interactions beyond the constant charging energy model give a Gaussian distribution of $\Delta_2(N)$ and increase the standard deviation of the addition spectra with respect to the constant charging energy approximation.^{5,7-11} These interactions are characterized by the ratio r_s between the direct Coulomb and the kinetic Fermi energies. The resulting standard deviation of the addition spectra includes a term due to the fluctuations of the single-particle spectra and a term arising from the fluctuations of the charging energy $E_C = e^2/C_\Sigma$. The former contribution is estimated for chaotic or diffusive dots from the random matrix theory (RMT): $\sigma_2 \approx 0.52\Delta_1$.⁵ For small ($r_s \ll 1$) or moderate values of r_s ,⁷ the latter is typically estimated as $\sigma_2 \approx \Delta_1(r_s/\sqrt{g_T})$, where $g_T \propto (e^2/h)(k_F\ell)$ is the local dimensionless 2D conductance in the dot.^{1,11} As a result $\sigma_2 \approx \Delta_1$, even after introducing spin¹⁰ or exchange¹ effects in the calculations. Smaller values of g_T result in a larger σ_2 .¹² In the case of very large r_s (negligible kinetic energy), one expects a Maxwell distribution, where the standard deviation scales as the charging energy ($\sigma_2 \propto E_C$).^{13,14}

We have analyzed the distribution of the addition energies as a function of the area of the quantum dot, restricting ourselves to the regime of large carrier densities in the dot. In contrast to previous experiments, we have studied the standard deviation of the addition spectra in low mobility silicon quantum dots obtained by resistive confinement from thin silicon-on-insulator (SOI) films.¹⁵ We find that the fluctuations of the addition energy scale as the inverse area of the dot. The fluctuations are comparable to the mean level spacing for the one-particle spectrum, in agreement with most recent theories.¹⁰

The devices were made from boron-doped (10^{15} cm^{-3}) SOI (100) wafers. In order to ensure a low resistivity for the electrical contact to the silicon, the silicon film lying under the contacts is thick (70 nm) and heavily doped. During doping, the active areas are protected from amorphization by a local thermal oxide layer. After its removal, we proceed to ion implantation (As ions above $10^{19} \text{ at. cm}^{-3}$) of the thin active areas (12–22 nm thick). A hybrid deep UV/electron-beam (e-beam) lithography combined with resist trimming is used to pattern silicon nanowires with width W in the range 20–400 nm and length L_f . After the silicon wires have been etched, a 4-nm-thick gate oxide was thermally grown before chemical vapor deposition of the *in situ*-doped poly-Si gate. E-beam lithography was then used to pattern gates with length L down to 40 nm. The backend sequence follows a standard complementary metal-oxide semiconductor (CMOS) process. Figure 1 shows a scanning electron micrograph (SEM) of the cross section of a typical wire.

The confinement of the dot is obtained by the part of

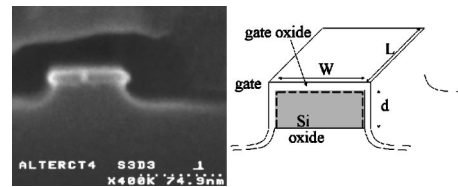


FIG. 1. (Left) SEM picture of a specific morphological characterization structure: Cross section of a 12-nm-thick and 60-nm-wide silicon nanowire. (Right) Layout of a sample showing the 2D electron gas (dash lines) of surface area $A = W \times L + 2 \times d \times L$.

TABLE I. Samples used in this study. W : wire width; L : gate length; L_f : wire length; d : wire thickness; $\langle\delta V_g\rangle$: average peak spacing in gate voltage at $T=4.2$ K; Δ_1 : one-particle mean level spacing. The dimensions are in nm.

	W	L	L_f	d	$\langle\delta V_g\rangle$ (mV)	Δ_1 (meV)
S1	70	40	200	12	3.8 ± 0.3	0.17
S2	50	40	200	17	5.9 ± 0.4	0.19
S3	70	80	200	22	2.8 ± 0.1	0.07
S4	50	80	200	22	3.7 ± 0.3	0.09
S5	40	60	100	22	5.6 ± 0.3	0.13
S6	50	40	200	22	5.9 ± 0.3	0.17
S7	100	100	200	22	2.1 ± 0.5	0.04
S8	70	40	200	22	6.7 ± 0.2	0.13

highly resistive SOI wire away from the gate. There is no deliberate oxidation of the silicon film to create tunnel barriers as in the pattern dependent oxidation (PADOX) process.¹⁶ We used neither fluctuations of the channel width to shape the quantum dot^{17–19} nor control gates to define the dot electrostatically. The latter procedure induces a deformation of the dot, which influences the addition spectra.^{6,20} The area and shape of our dots is simply given by the overlap between the gate and the SOI film; the area can be as low as 3300 nm² and as high as 14 400 nm². This results in values for Δ_1 , which are larger than in previous studies (see Table I).^{3–6}

A 2D electron accumulation layer is formed near the surface of the nanowire (see Fig. 1). The mobility was estimated from the sheet resistance of SOI films without gates. Under the gate it could be either enhanced, because of the protection provided by the gate, or decreased by electrostatic disorder at the gate oxide/poly-Si interface. From $r_{\square} \approx 4000 \Omega$ (at room temperature as well as at $T=4.2$ K, for $d=22$ nm) and the doping level, we estimate the mobility to be $\mu \approx 150 \text{ cm}^2 \text{ V}^{-1} \text{ s}^{-1}$ and $(k_F \ell) \approx 3-5$. $r_s = (a_{\text{Bohr}} \sqrt{\pi n_S})^{-1}$ is 0.6 for $n_S = 10^{13} \text{ cm}^{-2}$ (1.7 for $n_S = 10^{12} \text{ cm}^{-2}$).

Hundreds of samples with various geometries, doping, and gate oxide thicknesses were integrated on 200-mm wafers. We chose 20 samples to study at low temperature, which were cleaved and mounted in a He3/He4 dilution refrigerator with a working temperature range of $70 \text{ mK} < T < 4.2$ K. An ac drain-source voltage V_{DS} was applied and the I_{DS} current measured with a standard lock-in technique. Lossy microcoaxes were used for rf filtering. Due to the device variations (see Table I), we were able to adjust the access resistance to favor the observation of single-electron transport. Under these conditions the resistances varied little between $T=300$ K and $T=4.2$ K with values of the order of 100 k Ω measured at large gate voltage. This value is typical for having resistive confinement as demonstrated in Ref. 21 and analyzed in Ref. 22. The recorded features are remarkably stable, even after several cooling cycles. The statistics are obtained by single V_g scans covering several hundreds of peaks.

The inset of Fig. 2 shows a detail of a typical drain-source

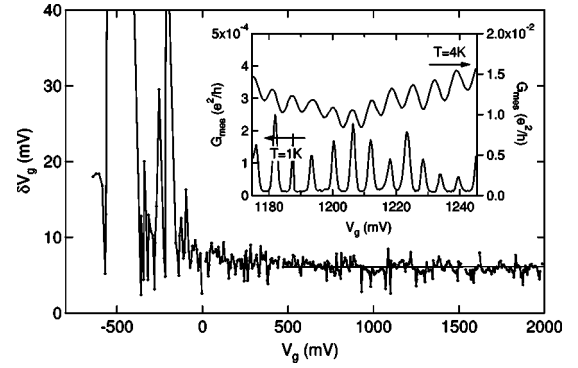


FIG. 2. Peak spacing δV_g vs gate voltage V_g of a Si-wire transistor (sample S6) at $T=4.2$ K. The inset shows typical conductance resonances as a function of V_g at $T=1$ K and $T=4.2$ K. For the statistics only the high V_g regime (many electrons) was considered, where δV_g is approximately constant [slope of linear fit (line): -10^{-4}].

conductance as a function of the gate voltage V_g . The spacings δV_g between the peaks for the whole gate voltage range are shown below the inset. Neglecting the first few dozen peaks, the mean value of the peak spacing in Fig. 2 is $\langle\delta V_g\rangle = 5.9 \pm 0.2$ mV. An overview of $\langle\delta V_g\rangle$ for different wire geometries is given in Table I. We have chosen samples with the same level of doping (10^{19} As/cm^3) and the same gate oxide thickness ($t_{ox}=4$ nm). The slope of a linear fit in the range $0.5 < V_g < 2$ V is of the order of 10^{-4} , indicating that the gate capacitance C_g is little affected by the increasing number of electrons in the dot.²³ This is in contrast with the observation of Ref. 19, where a shift of the period with gate voltage was attributed to an electrostatic coupling between two dots. We compared the measured values of $\langle\delta V_g\rangle$ with the expected values $\delta V_{cal} = e/C_g$ for a planar capacitance $C_g = \epsilon_r \epsilon_0 A/t_{ox}$, where A is the surface area of the 2D gas (see Fig. 1) and ϵ_r is the relative dielectric constant of the oxide. Figure 3 shows this ratio between measured and calculated

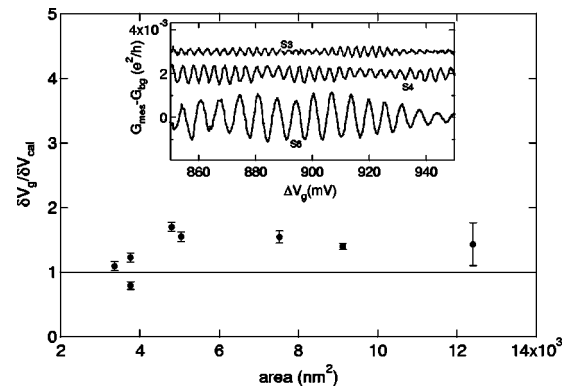


FIG. 3. Ratio of the measured (δV_g) and calculated (δV_{cal}) peak-to-peak distance for a flat capacitance $C = \epsilon_0 \epsilon_r A/t_{ox}$ ($\epsilon_r = 3.9$, area A , oxide thickness $t_{ox} = 4$ nm). The inset shows measured oscillations after subtraction of the background in units of e^2/h as a function of the gate voltage V_g for three different areas (lowest curve: sample S6; middle curve: sample S4; highest curve: sample S3). Curves for S4 and S3 were shifted for clarity.

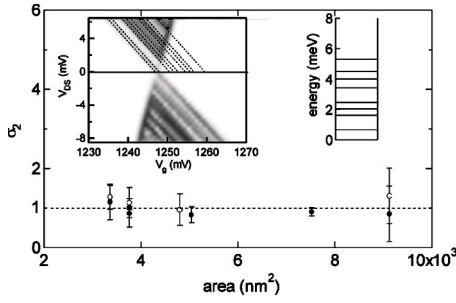


FIG. 4. Fluctuations of the peak spacing distributions σ_2 , normalized to the mean one-particle energy-level spacing Δ_1 vs area A (filled dots: 4.2 K, open dots: 1 K). The inset shows the typical $V_{DS}-V_g$ diamonds of the first-conductance peak in $A=3300 \text{ nm}^2$ sample. The one-particle levels appear as additional lines in the diamonds. Projecting along the V_g axis and taking $\alpha=0.4$ gives the measured excitation spectrum, with a mean value $\Delta_1=0.6\pm 0.2 \text{ meV}$, in good agreement with the calculated values of Table I (see text).

mean peak spacings for the samples listed in Table I. The ratios are close to 1, which show that the dot size is, indeed, close to the area A covered by the gate. We estimate the mean level spacing $\Delta_1 = \pi \hbar^2 / 2m^*A$ ($m^* = 0.19m_e$ is the effective mass of the electron), taking into account the spin and band degeneracy for electrons on the (100) silicon surface.²⁴ We compared this value with direct measurements of the excitation spectra in a sample of comparable size ($A = 3300 \text{ nm}^2$) but different doping from samples S1 to S7. For low carrier densities we find additional levels in the typical diamond-shaped $V_{DS}-V_g$ dependence shown in the inset of Fig. 4. The measurement of the level distances is in good quantitative agreement with the estimation of Δ_1 considering that, due to the so-called Lifschitz tail, Δ_1 is expected to be larger at lower densities, by roughly a factor of 2 or 3.²⁴

For the analysis of the distribution of Δ_2 we assumed a constant value for α , as in previous works, although it decreases slightly with V_g . This variation is enhanced at low V_g (in the first peaks region omitted from the statistics) because of the reduction of the source and drain capacitances. As usual in metal-oxide-semiconductor field-effect transistors (MOSFETs) near threshold, the capacitances between the channel and source/drain and body, respectively, increase with the gate voltage, while the gate capacitance remains constant.²⁵ α is obtained from the slopes of the Coulomb diamonds at intermediate gate voltages and by fitting the temperature dependence of the resonances at high gate voltage. $\alpha \approx 0.4$ is found for all samples from the analysis of the Coulomb diamonds. We also note that α can fluctuate from resonance to resonance around its mean value, an effect neglected here which deserves a more systematic study. Figure 5 shows the distribution of the peak spacings in gate voltage δV_g for three different areas. As shown in the inset of Fig. 3, the distributions shift to higher mean values of δV_g as the sample size decreases. At the same time a broadening of the distribution can be observed. The measurements were usually done at $T=4.2 \text{ K}$, i.e., $k_B T \gtrsim \Delta_1$. A comparison with measurements at lower temperature, $T=1 \text{ K}$ and $T=300 \text{ mK}$ (effective minimal electronic temperature), has

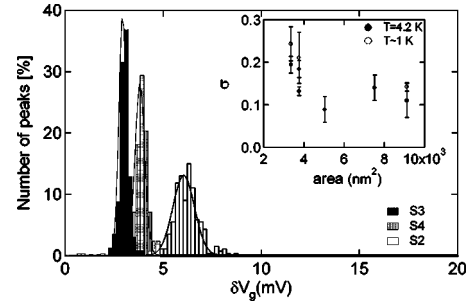


FIG. 5. Relative peak spacing distribution $P(\delta V_g)$ for three different dots' areas at 4.2 K. The solid lines are the Gaussian fits used to extract the standard deviation. The shift towards larger values of δV_g for decreasing areas is clearly visible. The distribution becomes larger when the sample area decreases. This enhancement of the fluctuations in smaller samples is shown in the inset, where the standard deviation σ of the normalized fluctuation $(\delta V_g - \langle \delta V_g \rangle) / \langle \delta V_g \rangle$ is plotted against the surface area of the sample.

shown that the addition spectra is slightly modified: σ_2 increases at lower temperature, but this increase lies within the error bars of the $T=4.2 \text{ K}$ statistics (see inset of Fig. 5). As in previous reports we observe a Gaussian distribution for the addition energies with a variance σ_2 , which is comparable to Δ_1 . The Gaussian shape contradicts the constant interaction approximation within the RMT model, where the ground-state energy is the sum of the charging energy and the energies of the occupied single-particle states.¹ To compare our results with theory,¹⁰ we plotted σ_2 normalized to Δ_1 as a function of the dots' area (see Fig. 4). Note that the simulation in Ref. 10 uses parameters comparable to ours: $r_S \approx 1.5$, $g_T \approx 4$, and $N \approx 200$. Due to the smaller size of our dots, Δ_1 is order of magnitudes larger than in Refs. 2 and 3. Alternatively, the inset of Fig. 5 shows the standard deviation σ of the frequently used normalization $(\delta V_g - \langle \delta V_g \rangle) / \langle \delta V_g \rangle$, obtained in Gaussian fits. The standard deviation increases when scaling down the area of the dots. σ reaches about 10% for the smallest sample ($A=3300 \text{ nm}^2$). This value is close to the ratio $\Delta_1 \sim 0.19 \text{ meV}$ over the value of the addition energy, $\Delta_2 = e\alpha \langle \delta V_g \rangle = 2.4 \text{ meV}$: $\Delta_1 / \Delta_2 = 0.08$. The normalization of σ_2 with Δ_1 (Fig. 4) leads to a constant σ_2 / Δ_1 (here ≈ 1), which proves that σ_2 scales with Δ_1 in our samples. At low gate voltages it is obvious from Fig. 2 that the fluctuations in σ_2 are greatly enhanced. We assumed that due to the low mobility of our samples and the low carrier concentration at low gate voltages, the electrons cross a mobility edge and the dot enters the localized regime. As the added electrons and their screening clouds are both localized on different sites, distant from almost zero to the diameter of the dot, the relative fluctuations of the addition spectra can reach 100% as explained in Ref. 13.

We presented a systematic study of the size dependence of the addition spectra in low mobility and ultrasmall silicon dots. Our dots are very similar to ultimate silicon MOSFETs, but different from those used in previous systematic experiments. The small size implicates a one-particle mean level spacing of the order of a few Kelvin, which is much larger than in previous experiments. Due to the chosen fabrication

technique, the dot shape is not modified by the gate voltage, which only modifies the concentration of electrons in the dot. We have found an excellent agreement with theories in the same range of parameters, both for the expected values and the size dependency of the fluctuations. The presented analysis is restricted to the high concentration range of carriers.

Experiments investigating the low-density case, where the dots undergo the metal-insulator transition, are in progress.

This work was partly supported by the European Commission under the frame of the Network of Excellence "SINANO" (Silicon-based Nanodevices, IST-506844).

*Electronic address: msanquer@cea.fr

¹Y. Alhassid and T. Rupp, Phys. Rev. Lett. **91**, 056801 (2003).
²S. R. Patel, S. M. Cronenwett, D. R. Stewart, A. G. Huibers, C. M. Marcus, C. I. Duruoz, J. S. Harris, K. Campman, and A. C. Gossard, Phys. Rev. Lett. **80**, 4522 (1998).
³F. Simmel, T. Heinzel, and D. A. Wharam, Europhys. Lett. **38**, 123 (1997).
⁴F. Simmel, David Abusch-Magder, D. A. Wharam, M. A. Kastner, and J. P. Kotthaus, Phys. Rev. B **59**, R10 441 (1999).
⁵U. Sivan, R. Berkovits, Y. Aloni, O. Prus, A. Auerbach, and G. Ben-Yoseph, Phys. Rev. Lett. **77**, 1123 (1996).
⁶S. Lüscher, T. Heinzel, K. Ensslin, W. Wegscheider, and M. Bichler, Phys. Rev. Lett. **86**, 2118 (2001).
⁷P. N. Walker, Y. Gefen, and G. Montambaux, Phys. Rev. Lett. **82**, 5329 (1999).
⁸R. Berkovits, Phys. Rev. Lett. **81**, 2128 (1998).
⁹D. Ullmo and H. U. Baranger, Phys. Rev. B **64**, 245324 (2001).
¹⁰H. Jiang, H. U. Baranger, and W. Yang, Phys. Rev. B **68**, 165337 (2003).
¹¹Ya. M. Blanter, A. D. Mirlin, and B. A. Muzykantskii, Phys. Rev. Lett. **78**, 2449 (1997).
¹²L. Bonci and R. Berkovits, Europhys. Lett. **47**, 708 (1999).
¹³A. A. Koulakov, F. G. Pikus, and B. I. Shklovskii, Phys. Rev. B **55**, 9223 (1997).

¹⁴A. A. Koulakov and B. I. Shklovskii, Phys. Rev. B **57**, 2352 (1998).
¹⁵X. Jehl, M. Sanquer, G. Bertrand, G. Guégan, S. Deleonibus, and D. Fraboulet, IEEE Trans. Nanotechnol. **2**, 308 (2003).
¹⁶Y. Takahashi, K. Kurihara, H. Iwadate, M. Nagase, and K. Murase, IEEE Trans. Electron Devices **43**, 1213 (1996).
¹⁷L. Zhuang, L. Guo, and S. Y. Chou, Appl. Phys. Lett. **72**, 1205 (1998).
¹⁸H. Ishikuro and T. Hiramoto, Appl. Phys. Lett. **71**, 3961 (1999).
¹⁹L. P. Rokhinson, L. J. Guo, S. Y. Chou, D. C. Tsui, E. Eisenberg, R. Berkovits, and B. L. Altshuler, Phys. Rev. Lett. **88**, 186801 (2002).
²⁰G. Hackenbroich, W. D. Heiss, and H. A. Weidenmüller, Phys. Rev. Lett. **79**, 127 (1997).
²¹V. A. Krupenin, A. B. Zorin, M. N. Savvateev, D. E. Presnov, and J. Niemeyer, J. Appl. Phys. **90**, 2411 (2001).
²²Y. V. Nazarov, Phys. Rev. Lett. **82**, 1245 (1999).
²³Nevertheless we take into account this variation of C_g to obtain the standard deviation σ_2 .
²⁴T. Ando, A. B. Fowler, and F. Stern, Rev. Mod. Phys. **54**, 437 (1982).
²⁵S. M. Sze, *Physics of Semiconductor Devices* (Wiley, New York, 1981).